First-Principles Evaluation of the Potential of Borophene as a Monolayer Transparent Conductor

Lyudmyla Adamska,[1] *Sridhar Sadasivam*,[2] *Jonathan J. Foley IV*,[3] *Pierre Darancet*,[2,‡] *and Sahar Sharifzadeh*[1,4,§]

[1] Department of Electrical and Computer Engineering, Boston University, Boston, Massachusetts 02215, United States

[2] Center for Nanoscale Materials, Argonne National Laboratory, Argonne, Illinois 60439, United States

[3] Department of Chemistry, William Paterson University, Wayne, New Jersey 07470, United States

[4] Division of Materials Science and Engineering and Department of Physics, Boston University, Boston, Massachusetts 02215, United States

CORRESPONDING AUTHORS FOOTNOTE: [‡] pdarancet@anl.gov, and [§] ssharifz@bu.edu

ABSTRACT

Two-dimensional boron is promising as a tunable monolayer metal for nano-optoelectronics. We study the optoelectronic properties of two likely allotropes of two-dimensional boron, β_{12} and δ_6, using first-principles density functional theory and many-body perturbation theory. We find that both systems are anisotropic metals, with strong energy- and thickness-dependent optical transparency and a weak (<1%) absorbance in the visible range. Additionally, using state-of-the-art methods for the description of the electron-phonon and electron-electron interactions, we show that the electrical conductivity is limited by electron-phonon interactions. Our results indicate that both structures are suitable as a transparent electrode.

KEYWORDS: borophene, two-dimensional materials, density functional theory, GW approximation, electron-phonon interactions

Introduction.

Two-dimensional (2D) boron or borophene is a recently synthesized[1–9] monolayer material predicted to exhibit novel thermal and optoelectronic properties,[10–14] that could complement other two-dimensional materials in creating new nanoelectronic devices. Borophene can exist in many different allotropes, all, while metallic, displaying distinct features of the band structure;[12–26] and has been predicted to form Ohmic contacts with other 2D semiconductors, suggesting that it can be a tunable monolayer metal.[27] Additionally, several reports have predicted phonon-mediated superconductivity in borophene,[22–26] which is very sensitive to carrier doping and strain,[25,26] and extremely low lattice thermal conductivity[28] compared with carbon-based materials[29]. To take advantage of borophene as a nano-optoelectronic material, it is necessary to understand its fundamental, intrinsic properties.

While borophene has been synthesized on metallic substrates, it has not yet been isolated and so most of the understanding of its optoelectronic properties arise from theory and computation. In particular, density functional theory (DFT) studies have probed the band structure of different borophene allotropes; these studies predict that different low-energy crystal structures may result in metallic or semi-metallic behavior,[30–33] may contain Dirac cones at or near the Fermi energy,[30–39] and display an in-plane anisotropy of conductivity due to their often anisotropic bonding configuration.[16,20] However, the understanding of the role of structure on borophene conductivity and optical properties is limited[19] and does not address optical transparency in particular. Moreover, to the best of our knowledge, the role of many-body effects on the optoelectronic properties, which is expected to be significant in other two-dimensional materials such as graphene,[40] has not been investigated previously.

In this letter, we investigate the electronic conductivity and optical transparency of two borophene allotropes, which have been previously suggested as likely structures experimentally grown on Ag(111) and display very different crystal structures (see Fig. 1). We perform state-of-the-art many-body perturbation theory (MBPT) calculations to describe electron-electron and electron-phonon interactions, in conjunction with rigorous electrodynamics simulations, to determine the spectral functions and optical behaviors of these two allotropes. We determine that these materials have a strongly temperature-dependent electronic conductivity that is a factor of

five smaller than graphene's at room temperature due to the strong electron-phonon scattering. In addition, they are weak absorbers with absorptivity of less than 1% in the visible range, resulting in excellent transparency. Moreover, we demonstrate that there is a transition from transparent to reflective metallic behavior in the visible for layered films, as the thickness is increased from ~ 1nm in the monolayer to ~20-30 nm in the film. Overall, we determine that either structure can serve as a complement to graphene as a metallic monolayer that is transparent in the visible range, but that their electronic conductivity is strongly dependent on atomic structure.

Results.

We investigate the electronic, vibrational, and optical properties of two monolayer boron allotropes: the δ_6 and β_{12} phases shown in Fig. 1. Both have been proposed[4,7,41] as possible structures grown on Ag(111) because of the close lattice match with the $1 \times \sqrt{3}$ substrate supercell of size 2.8 Å × 5 Å. The δ_6 structure was originally proposed in Ref.[41] as satisfying the periodicity of STM images, while β_{12} was later found as a more suitable candidate as fulfilling both short-range and long-range Moire patterns of the observed STM graphs.[42] Both structures[43] form a rectangular lattice; δ_6, with space group 59-Pmnm (D2h-13), contains two atoms per unit cell that are arranged in an out-of-plane corrugated fashion, as shown in Figs. 1a-b; and β_{12}, with space group 47-Pmmm (D2h-1), contains five atoms per unit cell. As shown in Figs. 1c-d, we study the 2×1 supercell of β_{12} in order to avoid calculations with an unpaired number of electrons.

We utilize DFT within the local density approximation (LDA[44,45]) and MBPT[46–50] to simulate the optoelectronic properties of the two boron allotropes. MBPT within the GW and Bethe-Salpeter equation (BSE) approach describes the long-range electron correlation and excitonic effects that may be important in describing the properties of low-dimensional materials.[40,51–54]

Fig. 1 shows the band structure of both allotropes, computed within both DFT and the GW approximation. Our DFT calculations agree well with previous local and semi-local DFT studies in the features of the band structure;[12–18,20–26,41,55] we predict that both borophene allotropes are metallic but that their band structures differ substantially. For δ_6, two bands cross the Fermi energy (E_F) at distinct locations in the Brillouin zone, with a noticeably wide gap of 4.3 eV in the

band structure at Γ (**k** = 0), while the β_{12} bandstructure displays many bands crossing E_F. Interestingly, the β_{12} band structure contains a set of linearly crossing bands reminiscent of the graphene Dirac point, at 0.6 eV above the Fermi energy near the Y-point of the band structure.

Comparison of DFT-LDA and GW band structures (shown in black and colored lines, respectively) reveals the role of many-body effects on the electronic structure of borophene. For the δ_6 allotrope, the GW correction to DFT-LDA eigenvalues are negligible near E_F and increase linearly away from E_F up to a magnitude of 100-200 meV. This is similar to the case of graphene where the GW correction is zero at the Dirac point and increases linearly in the vicinity of the K-point, saturating to a nearly constant value for the quadratic band at the M-point.[40,56] For the β_{12} allotrope, the GW corrections are small near E_F and increase up to an almost constant shift of 400 meV at 7 eV below E_F.

Interestingly, the GW correction to DFT increases the Fermi velocity of electrons by about 15-30% (depending on band index and position in Brillouin zone) for both borophene structures. As an example, for the two bands crossing the Fermi surface in the Γ-Y direction in the δ_6 structure, the DFT-calculated Fermi velocities are 0.54×10^6 m/s and 1.28×10^6 m/s while GW velocities are 0.66×10^6 m/s and 1.51×10^6 m/s. Similarly, for the β_{12} structure, two representative DFT-calculated Fermi velocities of 0.66×10^6 m/s (Y-S direction) and 0.89×10^6 m/s (S-Γ direction) increase to 0.87×10^6 m/s and 1.18×10^6 m/s, respectively, with GW. The Fermi velocities in borophene are typically smaller but of the same order of magnitude as that of graphene which is $\sim 1.1 \times 10^6$ m/s, although, along certain directions in the Brillouin zone (e.g., 1.51×10^6 m/s along the Γ-Y direction in δ_6 and 1.18×10^6 m/s along S-Γ direction in β_{12}), the Fermi velocities are larger than those of graphene. Similar to the present predictions for borophene, GW-renormalization of the band structure has been predicted to increase the Fermi velocity in graphene by about 17% in comparison to DFT LDA.[56]

Figs. 1e-f and 2c-f present the electron linewidths resulting from electron-phonon scattering within these structures, which were calculated using the Electron-Phonon Wannier (EPW) package.[49,57,58] The color map in Fig. 1e-f shows the strength of electron-phonon interactions associated with the GW-corrected quasiparticle states. We find that electron linewidths for δ_6 borophene are generally smaller than for β_{12}, associated with the weaker Fermi surface nesting

caused by the smaller number of metallic bands. Figs. 2c-f show the electron linewidth for all states within a window of 1.5 eV around E_F. The peaks in the linewidth closely follow the peaks in the density of states DOS (Figs. 2a,b) since an increase in DOS also increases the phase space for electron-phonon scattering and the corresponding self-energy. The shift in the peak positions of the linewidth (see Figs. 2c,e at 1eV below E_F) between DFT and GW also closely follow the corresponding shifts in DOS (Fig. 2a) due to GW renormalization of the bandstructure.

At very low temperatures (10K), we predict the electron linewidth for δ_6 borophene to be zero at E_F and increase linearly up to 70 meV for $|E-E_F| = 0.25$ eV as shown in Fig. 2c. At room temperature (300K), the linewidth increases to 20 meV at E_F and again increases by 70 meV for up to 0.25 eV away from E_F. Beyond this energy range, there are large fluctuations in the linewidth, with unoccupied states fluctuating in the range of 40-70 meV and occupied states fluctuating in the range of 40-150 meV, and maximal value of 150 meV at about 1 eV below E_F.

The β_{12} allotrope shows a stronger temperature dependence of its electron linewidth in comparison to the δ_6 allotrope. Similar to δ_6, at low temperatures the linewidth is near zero at E_F and increases linearly up to $|E-E_F| < 0.2$ eV, saturating at ~75 meV for unoccupied states and ~100 meV for occupied states as shown in Fig. 2d. At room temperature (Fig. 2f), we predict large linewidths up to 300 meV where low-frequency unstable phonon modes were found to contribute significantly to electron-phonon scattering (see also discussion on electronic conductivity below).

The general features of the electronic state broadening are similar to graphene for both allotropes, which also shows linear increase around Fermi energy.[59] However, the linewidth in graphene around E_F is significantly smaller than in borophene; the maximum linewidth in graphene for states at 1 eV around the Fermi level is 30 meV at 300 K (see Fig. S3.2), while both allotropes of borophene have maximum linewidths of 200-300 meV (see Figs. 2e,f) at the same temperature. This is because of the significantly weaker electron-phonon interactions in graphene; the electron-phonon coupling constant in graphene[57] is around 0.5, substantially weaker than in borophene ~0.6-0.7 in the β_{12}[22,23] and 1.1 in the δ_6[22] structure. This results in a significantly reduced electron relaxation time. For example, we predict that the electron-phonon relaxation time averaged around the Fermi energy for n-doped graphene with a carrier

concentration of 3.9 x 10^{13} cm^{-2} is 650 fs at 300 K (see Fig. S3.2). The corresponding relaxation times for the δ_6 and β_{12} allotropes are predicted to be 7 fs and 4 fs respectively.

Such large electron-phonon interactions in borophene result in lowered finite temperature conductivity due to scattering. Figs. 2g-h present the calculated electronic conductivities within DFT-LDA. The β_{12} allotrope is unstable[22] as a freestanding monolayer resulting in phonon dispersion that contains imaginary modes (see Fig. S3.1) that are found to significantly scatter with electrons. In practice, such instabilities are expected to be stabilized through strain or charge transfer from the substrate.[22] Hence, we report a wide conductivity range for the β_{12} allotrope in Fig. 2h where the lower limit to the conductivity considers scattering of electrons with all phonon modes while the upper limit considers only scattering with phonons of energies greater than 25 meV. The choice of phonon energy cutoff is guided by the extent of imaginary phonon branches (see Fig. S3.1). For comparison, we also include the conductivity for n-doped graphene with a carrier concentration of 3.9×10^{13} cm^{-2} where the Fermi level is at 0.6 eV above the Dirac point.

The important properties that determine electrical conductivity are the Fermi velocity, DOS at E_F, and the electron-phonon relaxation time near E_F. While the electron-phonon relaxation time in borophene is about two orders-of-magnitude smaller than that in graphene, the DOS at E_F is almost one order-of-magnitude larger in borophene as compared to n-doped graphene (~ 0.01 states/eV/spin/atom in graphene vs. ~ 0.1 states/eV/spin/atom in borophene) due to the metallic nature of borophene. The Fermi velocities in graphene and borophene are of similar magnitudes as described earlier. Thus, the DFT-calculated conductivity in borophene is about one order-of-magnitude smaller than in graphene.

An additional distinction between borophene and graphene is the highly anisotropic nature of the borophene crystal structure, which leads to anisotropy in the electrical conductivity. For the δ_6 allotrope, the conductivity in the y-direction is about 2-3 times larger than that in the x-direction. Such anisotropy is to be expected based on the bandstructure (see Fig. 1e), which contains two bands cross the Fermi surface along the Γ-Y direction while no bands cross the Fermi energy in the Γ-X direction. In contrast, the β_{12} allotrope has many bands crossing the Fermi surface in all directions (see Fig. 1f) and does not show any anisotropy in electrical conductivity. Our

prediction primarily shows that stabilization of the β_{12} allotrope through strain or charge transfer is expected to enhance its conductivity close to graphene. The GW corrections to the conductivity are expected to be small since the corrections to DOS and group velocity at the Fermi energy are in opposite directions, i.e., Fermi DOS is slightly over-estimated in the DFT bandstructure (Figs. 2a,b) while the Fermi velocity is under-predicted by 15-30% as described earlier.

Next, we investigate the optical properties of borophene and its potential as a transparent electrode. Our MBPT calculations predict that exciton binding energies are 25 meV and 5 meV for δ_6 and β_{12} boron allotropes, respectively, indicating that the random phase approximation (RPA), which neglects excitonic effects, is sufficient for describing this system. Fig. 3 shows the RPA-calculated optical absorption calculated from the real ε_1 and imaginary ε_2 part of the dielectric function, both of which are dependent on the polarization of incoming light.[55] We predict that ε_1 diverges at an energy of 2.94 eV (2.33 eV) and 2.02 eV (3.83 eV) for X- (Y-) polarized light within the β_{12} and δ_6 allotropes, respectively (Fig. 3c-d), suggesting a strong electronic response at these energies. ε_2 shows a similar anisotropy in response to light polarization direction, particularly for the δ_6 allotrope (Fig. 3e-f); for this structure, the onset of ε_2 occurs at 2 eV and 3 eV for X- and Y-polarized light, respectively, with a peak at 2.6 eV and 6.2 eV for X and Y polarizations.

The absorbance in both allotropes is quite weak, absorbing less than 1% of incident light in the visible region (Figs. 3a-b), which is weaker than that of graphene (2.3%).[60] The δ_6 allotrope is predicted to have a gap in optical absorption at 2.6 eV, which corresponds to transitions from partially occupied bands along the Γ-Y direction (Figs. 1e and S2.2), while for β_{12}, the onset of absorption is at 0.4 eV which corresponds to transitions in the vicinity of the Γ -point (Figures 1f and S4.4).

In order to understand optical transparency, we compute reflection and transmission by numerically solving the Maxwell's equations for a material of a given thickness with the RPA-calculated $\varepsilon_{1,2}$. In order to better understand the role of low-dimensionality, we increase the material thickness from 7 Å, an estimate for the monolayer, up to 350 nm, which approximates the semi-infinite bulk limit as shown in Fig. 4. For both structures, the monolayer borophene is

highly transparent at nearly all energies (beyond 0.1 eV) for both X- and Y- polarized light. In contrast, at the semi-infinite limit, the material is highly reflecting at these energies. Our analysis shows that analysis of reflectivity and transmittance for the semi-infinite, such as when using the Fresnel equations, is not appropriate for the monolayer. The high-reflectivity in the semi-infinite limit is due to the metallic character of the borophene; however, high visible reflectivity is not observed when the thickness is much smaller than the skin depth, which explains the high transmissivity of monolayers of both allotropes. Interestingly, there is a continuous change in the transmittance profile with thickness, with the region of transparency getting smaller and moving to higher energies as the thickness is increased. In both boron allotropes, at all thicknesses, there is increased transparency for X-polarized light in the UV-visible range of energies (500-600 nm in δ_6) and (350-400 nm in β_{12}). The transparency peaks (see Fig. 4) arise because the imaginary part of the refractive of the index approaches zero, resulting in nearly perfect transmission of the incident wave.

Conclusions.

In summary, we employed density functional theory and many-body perturbation theory to understand the optoelectronic properties of two likely phases of monolayer boron. We determined that both allotropes are transparent metals in the visible range with weak many-body interactions and strong electron-phonon interactions that limit their conductivity. Our study indicates that borophene can function as a transparent electrode and will complement graphene in the library of possible two-dimensional materials for optoelectronic devices.

Computational details.

Density Functional Theory (DFT) and Random Phase Approximation (RPA) calculations were performed using Quantum Espresso[61] simulation suite with norm-conserving Troullier-Martins[62] pseudopotentials within the local density approximation (LDA). Wave function cutoff was to 100 Ry, which converged the total energy to less than 1 meV/atom. The K-point grid for δ_6 and β_{12} cells were $24 \times 40 \times 1$ and $12 \times 14 \times 1$, respectively, which ensure the convergence of total DFT energy to 10^{-3} eV accuracy. The k-point density was $2\pi \times 0.015$ Å^{-1} for band structure

calculations and was decreased $2\pi \times 0.003$ Å^{-1} for RPA calculations in order to obtain a smooth dielectric function.

The unit cell sizes of two boron structures were geometry optimized with force convergence criterion of 10^{-5} eV/Å. The size of δ_6 unit cell was 2.829×1.606 and out-of-plane rumpling was 0.828 Å. The relaxed unit cell size of β_{12} boron structure is 2.892×4.995 Å. The calculated work functions of δ_6 and β_{12} boron allotropes are 5.535 eV and 5.227 eV, respectively.

MBPT simulations were performed for δ_6 and β_{12} using the BerkeleyGW[50] MBPT package. For both allotropes, the perpendicular dimension of the unit cell was set to 20 Å, which converged the Fermi energy to better than 0.001 eV within DFT-LDA. In order to minimize spurious interactions due to periodic boundary conditions, the Coulomb potential was truncated at half of the unit cell length. The number of empty states included in the GW sum was 800 for both structures, spanning an energy range of 240 eV and 68 eV for the δ_6 and β_{12} structures, respectively. The planewave cutoff for the dielectric matrix was 6 Ry; increasing the cutoff to 12 Ry resulted in change of eigenvalues of less than 0.1 eV. 30 and 60 bands were included in BSE summation for δ_6 and β_{12} borophene structures, respectively.

Electron-phonon interactions and electron linewidths were evaluated from electron-phonon matrix elements computed using Wannier interpolation within the EPW package.[57,58] Electron-phonon matrix elements were computed on coarse k- and q-grids using density functional perturbation theory (DFPT) within Quantum Espresso and interpolated to fine k- and q-grids needed for convergence of electron self-energies. DFPT calculations were performed using coarse q-grids of $12 \times 20 \times 1$ and $6 \times 7 \times 1$ for δ_6 and β_{12} structures, respectively. Electron self-energies were computed using fine q-grids of $72 \times 120 \times 1$ (δ_6) and $90 \times 100 \times 1$ (β_{12}). For electron self-energies using the GW band structure, the same procedure and grid sizes were used except that Wannier interpolation was performed using the GW quasiparticle energies instead of DFT (phonons and electronic wavefunctions were still computed within the DFT formalism). A similar procedure was followed for graphene where DFPT calculations were performed on a $24 \times 24 \times 1$ q-grid with a coarse k-grid of $72 \times 72 \times 1$. Electron-phonon self-energies were computed through Wannier interpolation of scattering matrix elements to a fine q-grid of $400 \times 400 \times 1$ under LDA-DFT.

The electrical conductivity was computed from the DFT band structure for both δ_6 and β_{12} structures using the BoltzWann package[63] under the relaxation time approximation. The conductivity tensor σ_{ij} is given by:

$$\sigma_{ij} = e^2 \int_{-\infty}^{+\infty} \left(-\frac{\partial f(E,\mu,T)}{\partial E} \right) \Sigma_{ij}(E) dE$$

where $\Sigma_{ij}(E) = \frac{1}{V} \sum_{nk} v_i(n,k)\, v_j(n,k) \tau_{nk} \delta(E - E_{nk})$ is the transport distribution function, $v_i(n,k)$ denotes the group velocity along direction 'i' and τ_{nk} denotes the electron-phonon relaxation time. At each temperature, the imaginary part of the electron self-energy due to electron-phonon interactions ($Im(\Sigma_{e-ph})$) was used to compute the electron-phonon relaxation time ($\tau_{e-ph} = \frac{\hbar}{2\Sigma_{e-ph}}$) for electronic states around the Fermi energy. A single Fermi-window averaged relaxation time was then used in the calculation of electrical conductivity and electronic velocities were obtained using Wannier interpolation in the BoltzWann package. Fine k-grids of $96 \times 160 \times 1$ (δ_6), $120 \times 140 \times 1$ (β_{12}) and $160 \times 160 \times 1$ (graphene) were used in Brillouin zone integration for calculation of electrical conductivity.

We compute the absorbance[64] from the imaginary component of the dielectric function, $A = \frac{\omega}{c} \epsilon_2 L$, where L is the dimension of the unit cell, perpendicular to borophene plane, ω is the energy of incident light, and c is the speed of light.

The normal-incidence optical transmission (T) and reflection (R) of borophene were computed by solving the Transfer Matrix equations.[65] In this approach, borophene is assumed to be a homogeneous medium with infinite extent in the $x - y$ plane and thickness d along z bounded above and below by air. Borophene is characterized by the isotropic dielectric function $\epsilon(\omega) = \epsilon_{xx}(\omega)$ to compute R and T for light polarized along x, and by the isotropic dielectric function $\epsilon(\omega) = \epsilon_{yy}(\omega)$ for light polarized along y. Because we consider only normal incidence, there is no polarization component along z, so $\epsilon_{zz}(\omega)$ does not play a role in the optical response. We validate this isotropic Transfer Matrix Method approach against an implementation of the full, anisotropic Transfer Matrix Equations[66] and find that the normal incidence reflection and transmission agrees to within numerical precision (see Figure S5.1).

The open-source package EMPy[67] was used to solve the anisotropic Transfer Matrix equations, where again, borophene is characterized as a medium of infinite extent in the $x-y$ plane with thickness d along the z, but in this case, the anisotropic dielectric tensor of the δ_6 phase from RPA is used to define the material. A detailed description of the isotropic and anisotropic Transfer Matrix Equations can be found in Refs.[65] and [66], respectively.

We validate our calculated thickness-dependent reflectivity and transmissivity of the δ_6 phase using by numerically solving Maxwell's equations in the $x-z$ plane containing the polarization and propagation vectors of the incident electric field, respectively. In particular, we compare broadband reflectance for light polarized along x from these simulations to our results from solving the isotropic Transfer Matrix equations for light polarized along x (see Figure S5.2). To elucidate the transition from the highly-reflective to highly-transmissive regime, we also compute the frequency-resolved electric field distributions for various δ_6 borophene thicknesses at 563 nm and 653 nm, which correspond to wavelengths that are highly transparent and highly reflective in the semi-infinite limit, respectively (see Figure S5.3). A commercial Simulator based on the finite-difference time-domain method was used to perform these calculations.[68] A non-uniform mesh was used to provide a high-resolution representation of the borophene monolayer, which was modelled as 1 nm thick layer film a grid size of 0.1 nm in x and z. A multi-coefficient model was fit the to δ_6 $\epsilon_{xx}(\omega)$ data between 500 and 5000 nm, providing an excellent fit to the RPA data across the bandwidth of the field source in the simulation. Anti-symmetric boundary conditions were employed along the x direction (the polarization direction of the electric field), and absorbing boundary conditions, i.e. perfectly matched layers, were employed along the z direction (the propagation direction of the electric field).

ACKNOWLEDGMENTS

The authors acknowledge the computational resources through Center for Nanomaterials at Argonne National Laboratory user program; the Extreme Science and Engineering Discovery Environment (XSEDE), which is supported by National Science Foundation grant number ACI-1548562, and the National Energy Research Scientific Computing Center, a DOE Office of Science User Facility supported by the Office of Science of the U.S. Department of Energy under Contract No. DE-AC02-05CH11231. L.A. acknowledges financial support from the BUnano postdoctoral fellowship. J.J.F. acknowledges financial support through the Center for Research at William Paterson University, College of Science and Health. Use of the Center for Nanoscale Materials, an Office of Science user facility, was supported by the U. S. Department of Energy, Office of Science, Office of Basic Energy Sciences, under Contract No. DE-AC02-06CH11357. S. Sadasivam was supported by Laboratory Directed Research and Development (LDRD) funding from Argonne National Laboratory. S. Sharifzadeh acknowledges financial support from the Early Career Award by the U.S. Department of Energy (DOE), Office of Science, Basic Energy Sciences (BES) Early Career Program under Award #DE-SC0018080.

AUTHOR INFORMATION

Lyudmyla Adamska: milaa@bu.edu
Sridhar Sadasivam: sadasivam@anl.gov
Jonathan J. Foley IV: foleyj10@wpunj.edu
Pierre Darancet: pdarancet@anl.gov
Sahar Sharifzadeh: ssharifz@bu.edu

SUPPORTING INFORMATION

Supporting information document contains auxiliary figures.

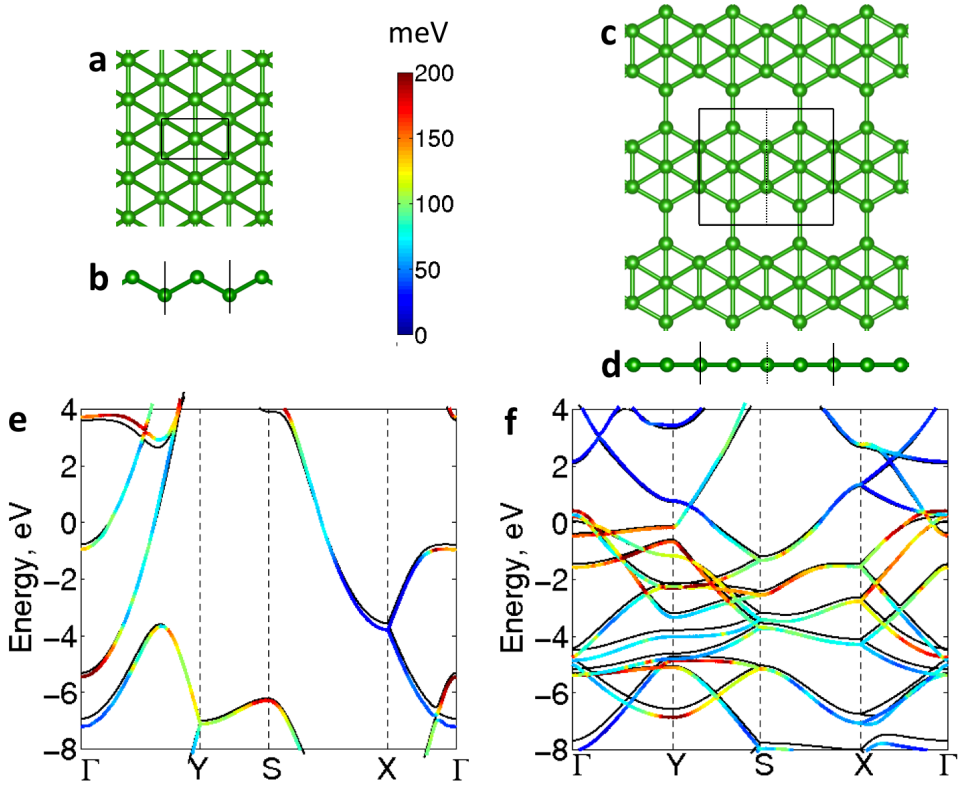

Figure 1. (a-d) The atomic structure of the δ_6 (a, b) and β_{12} (c, d) borophene allotropes. The solid lines show the periodically-repeating encloses 2x1 supercell used in this work. (e-f) The GW- (colored lines) and DFT- (black lines) predicted band structure of δ_6 (e) and β_{12} (f) boron allotropes. The band structure is shifted such that Fermi level is at zero energy and he GW eigenvalues are color-coded by the strength of electron-phonon interactions (meV).

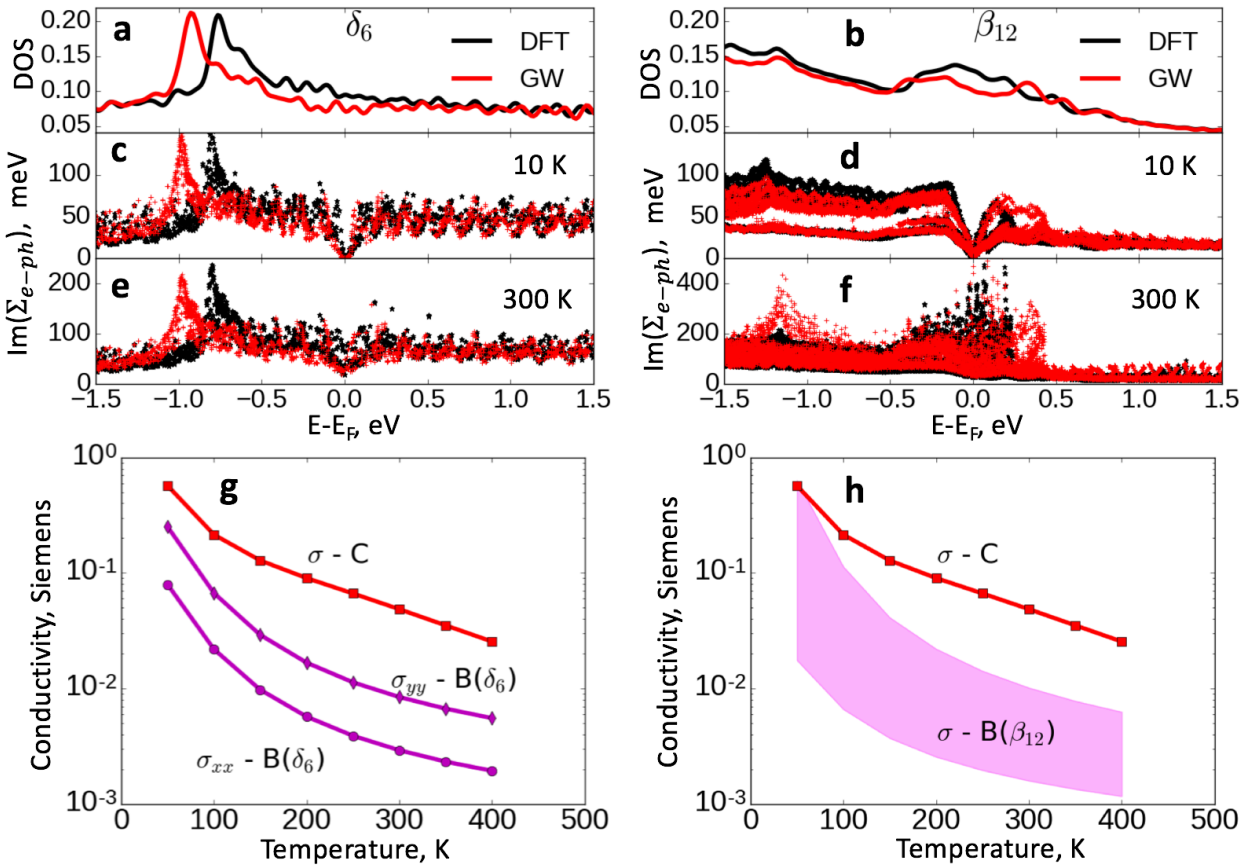

Figure 2. Electronic DOS (in units of states/eV/spin/atom) for δ_6 (a) and β_{12} (b) structures. Electron linewidth due to electron-phonon interaction for δ_6 (c, e) and β_{12} (d, f) allotropes at 10 K and 300 K. Temperature-dependent electrical conductivity σ of δ_6 (g) and β_{12} (h) borophene in comparison to graphene (labeled as C).

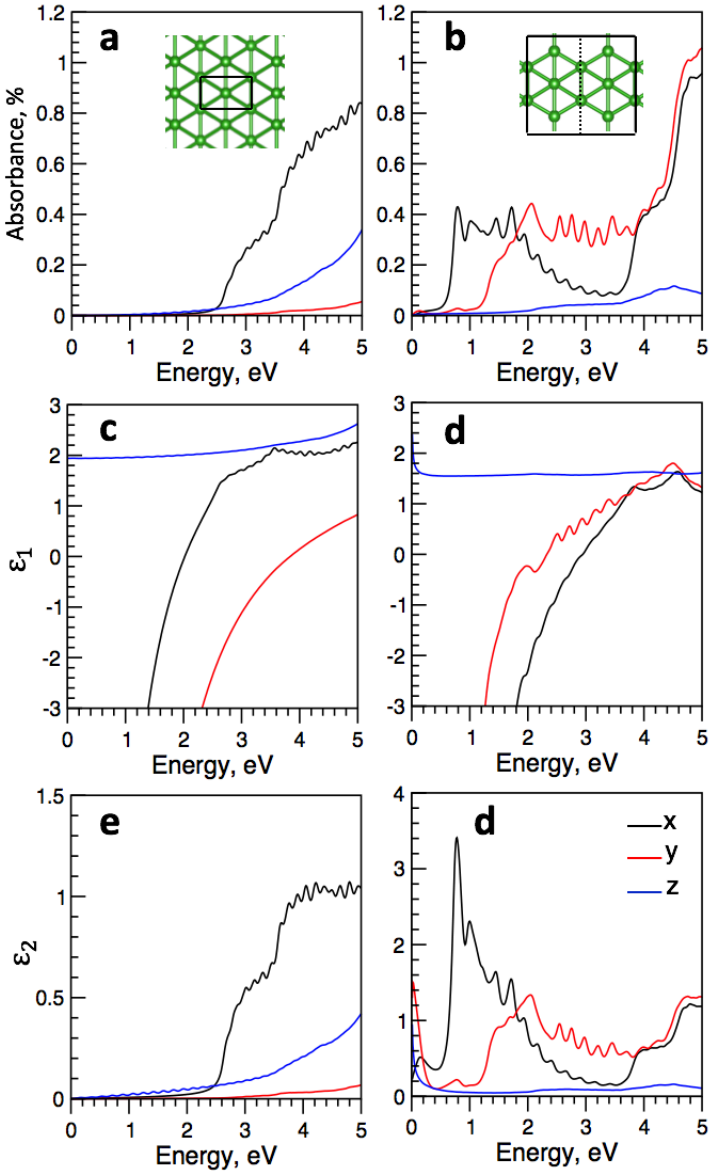

Figure 3. The calculated absorbance and real and imaginary component of the dielectric function for δ_6 and β_{12} borophene allotropes. The black, red, and blue colors correspond to x, y, and z polarizations of light.

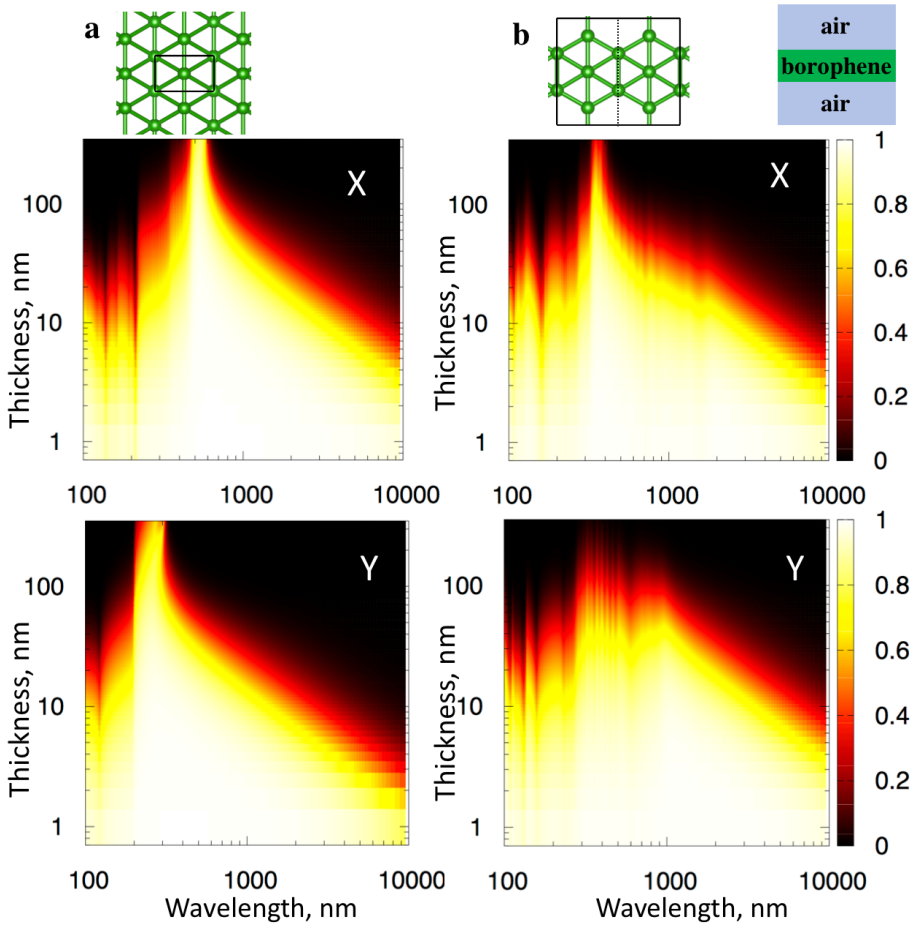

Figure 4. Calculated transmittance in (a) δ_6 and (b) β_{12} borophene films as a function of film thickness. The top panel shows transmittance for X-polarized light and the bottom for Y-polarized light.

REFERENCES

1. Tai, G., Hu, T., Zhou, Y., Wang, X., Kong, J., Zeng, T., You, Y. & Wang, Q. Synthesis of Atomically Thin Boron Films on Copper Foils. *Angew. Chemie Int. Ed.* **54,** 15473–15477 (2015).

2. Mannix, A. J., Zhou, X.-F., Kiraly, B., Wood, J. D., Alducin, D., Myers, B. D., Liu, X., Fisher, B. L., Santiago, U., Guest, J. R., Yacaman, M. J., Ponce, A., Oganov, A. R., Hersam, M. C. & Guisinger, N. P. Synthesis of borophenes: Anisotropic, two-dimensional boron polymorphs. *Science (80-.).* **350,** 1513–1516 (2015).

3. Zhong, Q., Kong, L., Gou, J., Li, W., Sheng, S., Yang, S., Cheng, P., Li, H., Wu, K. & Chen, L. Synthesis of borophene nanoribbons on Ag(110) surface. *Phys. Rev. Mater.* **1,** 21001 (2017).

4. Feng, B., Zhang, J., Zhong, Q., Li, W., Li, S., Li, H., Cheng, P., Chen, L., Wu, K., Meng, S., Chen, L. & Wu, K. Experimental Realization of Two-Dimensional Boron Sheets. *Nat Chem* **8,** 563–568 (2016).

5. Feng, B., Zhang, J., Liu, R. Y., Iimori, T., Lian, C., Li, H., Chen, L., Wu, K., Meng, S., Komori, F. & Matsuda, I. Direct evidence of metallic bands in a monolayer boron sheet. *Phys. Rev. B - Condens. Matter Mater. Phys.* **94,** 2–6 (2016).

6. Zhong, Q., Zhang, J., Cheng, P., Feng, B., Li, W., Sheng, S., Li, H., Meng, S., Chen, L. & Wu, K. Metastable phases of 2D boron sheets on Ag(1 1 1). *J. Phys. Condens. Matter* **29,** 95002 (2017).

7. Liu, X., Wei, Z., Balla, I., Mannix, A. J., Guisinger, N. P., Luijten, E. & Hersam, M. C. Self-assembly of electronically abrupt borophene/organic lateral heterostructures. *Sci. Adv.* **3,** e1602356 (2017).

8. Sun, X., Liu, X., Yin, J., Yu, J., Li, Y., Hang, Y., Zhou, X., Yu, M., Li, J., Tai, G. & Guo, W. Two-Dimensional Boron Crystals: Structural Stability, Tunable Properties, Fabrications and Applications. *Adv. Funct. Mater.* (2016). doi:10.1002/adfm.201603300

9. Tsai, H. S., Hsiao, C. H., Lin, Y. P., Chen, C. W., Ouyang, H. & Liang, J. H. Fabrication of Multilayer Borophene on Insulator Structure. *Small* 5251–5255 (2016). doi:10.1002/smll.201601915

10. Evans, M. H., Joannopoulos, J. D. & Pantelides, S. T. Electronic and mechanical properties of planar and tubular boron structures. *Phys. Rev. B - Condens. Matter Mater. Phys.* **72,** 1–6 (2005).

11. Kunstmann, J. & Quandt, A. Broad boron sheets and boron nanotubes: An ab initio study of structural, electronic, and mechanical properties. *Phys. Rev. B* **74,** 35413 (2006).

12. Tang, H. & Ismail-Beigi, S. Novel precursors for boron nanotubes: The competition of two-center and three-center bonding in boron sheets. *Phys. Rev. Lett.* **99,** 12–15 (2007).

13. Tang, H. & Ismail-Beigi, S. Self-doping in boron sheets from first principles: A route to structural design of metal boride nanostructures. *Phys. Rev. B - Condens. Matter Mater. Phys.* **80,** 1–8 (2009).

14. Tang, H. & Ismail-Beigi, S. First-principles study of boron sheets and nanotubes. *Phys. Rev. B - Condens. Matter Mater. Phys.* **82,** 1–20 (2010).

15. Massote, D. V. P., Liang, L., Kharche, N. & Meunier, V. Electronic, vibrational, Raman, and scanning tunneling microscopy signatures of two-dimensional boron nanomaterials. *Phys. Rev. B - Condens. Matter Mater. Phys.* **94,** 1–9 (2016).

16. Tsafack, T. & Yakobson, B. I. Thermomechanical analysis of two-dimensional boron monolayers. *Phys. Rev. B - Condens. Matter Mater. Phys.* **93,** 1–7 (2016).

17. Sun, H., Li, Q. & Wan, X. G. First-principles study of thermal properties of borophene. *Phys. Chem. Chem. Phys.* **18,** 14927–14932 (2016).

18. Peng, B., Zhang, H., Shao, H., Ning, Z., Xu, Y., Ni, G., Lu, H., Zhang, D. W. & Zhu, H. Stability and strength of atomically thin borophene from first principles calculations. *Mater. Res. Lett.* **5,** 399–407 (2017).

19. Peng, B., Zhang, H., Shao, H., Xu, Y., Zhang, R. & Zhu, H. The electronic, optical, and thermodynamic properties of borophene from first-principles calculations. *J. Mater. Chem. C* **4,** 3592–3598 (2016).

20. Cui, Z.-H., Jimenez-Izal, E. & Alexandrova, A. N. Prediction of Two-Dimensional Phase of Boron with Anisotropic Electric Conductivity. *J. Phys. Chem. Lett.* **8,** 1224–1228 (2017).

21. Sheets, T. B. M., Wu, X., Dai, J., Zhao, Y., Zhuo, Z., Yang, J. & Zeng, X. C. Two-dimensional boron monolayer sheets. *ACS Nano* **6,** 7443–7453 (2012).

22. Penev, E. S., Kutana, A. & Yakobson, B. I. Can Two-Dimensional Boron Superconduct? *Nano Lett.* **16,** 2522–2526 (2016).

23. Gao, M., Li, Q.-Z., Yan, X.-W. & Wang, J. Prediction of phonon-mediated superconductivity in borophene. *Phys. Rev. B* **95,** 24505 (2017).

24. Zhao, Y., Zeng, S. & Ni, J. Phonon-mediated superconductivity in borophenes. *Appl. Phys. Lett.* **108,** 242601 (2016).

25. Cheng, C., Sun, J.-T., Liu, H., Fu, H.-X., Zhang, J., Chen, X.-R. & Meng, S. Suppressed superconductivity in substrate-supported β_{12} borophene by tensile strain and electron doping. *2D Mater.* **4,** 25032 (2017).

26. Xiao, R. C., Shao, D. F., Lu, W. J., Lv, H. Y., Li, J. Y. & Sun, Y. P. Enhanced superconductivity by strain and carrier-doping in borophene: A first principles prediction. *Appl. Phys. Lett.* **109,** 1–6 (2016).

27. Liu, L. Z., Xiong, S. J. & Wu, X. L. Monolayer borophene electrode for effective elimination of both the Schottky barrier and strong electric field effect. *Appl. Phys. Lett.* **109,** 61601 (2016).

28. Xiao, H., Cao, W., Ouyang, T., Guo, S., He, C. & Zhong, J. Lattice thermal conductivity of borophene from first principle calculation. *Sci. Rep.* **7,** 45986 (2017).

29. Balandin, A. A. Thermal Properties of Graphene , Carbon Nanotubes and Nanostructured Carbon Materials. 1–37 (2011).

30. Zhou, X.-F., Dong, X., Oganov, A. R., Zhu, Q., Tian, Y. & Wang, H.-T. Semimetallic Two-Dimensional Boron Allotrope with Massless Dirac Fermions. *Phys. Rev. Lett.* **112,** 85502 (2014).

31. Carrete, J., Li, W., Lindsay, L., Broido, D. A., Gallego, L. J. & Mingo, N. Physically founded phonon dispersions of few-layer materials and the case of borophene. *Mater. Res. Lett.* **3831,** 1–8 (2016).

32. Zabolotskiy, A. D. & Lozovik, Y. E. Strain-induced pseudomagnetic field in the Dirac semimetal borophene. *Phys. Rev. B - Condens. Matter Mater. Phys.* **94,** 1–6 (2016).

33. Lopez-Bezanilla, A. & Littlewood, P. B. Electronic properties of 8- Pmmn borophene. *Phys. Rev. B - Condens. Matter Mater. Phys.* **93,** 2–6 (2016).

34. Xu, L.-C., Du, A. & Kou, L. Hydrogenated borophene as a stable two-dimensional Dirac material with an ultrahigh Fermi velocity. *Phys. Chem. Chem. Phys.* **18,** 27284–27289 (2016).

35. Wang, Z., Lü, T., Wang, H., Feng, Y. P. & Zheng, J. High anisotropy of fully hydrogenated borophene. *Phys. Chem. Chem. Phys.* **18,** 31424–31430 (2016).

36. Wang, Z., Lü, T., Wang, H. & Feng, Y. P. New crystal structure prediction of fully hydrogenated borophene by first principles calculations. 1–11 (2017). doi:10.1038/s41598-017-00667-x

37. Kou, L., Ma, Y., Tang, C., Sun, Z., Du, A. & Chen, C. Auxetic and Ferroelastic Borophane: A Novel 2D Material with Negative Possion's Ratio and Switchable Dirac Transport Channels. *Nano Lett.* acs.nanolett.6b04180 (2016). doi:10.1021/acs.nanolett.6b04180

38. Zhou, X.-F. & Wang, H.-T. Low-dimensional boron: searching for Dirac materials. *Adv. Phys. X* **6149,** 1–13 (2016).

39. Ma, F., Jiao, Y., Gao, G., Gu, Y., Bilic, A., Chen, Z. & Du, A. Graphene-like Two-Dimensional Ionic Boron with Double Dirac Cones at Ambient Condition. *Nano Lett*. **16,** 3022–3028 (2016).

40. Yang, L., Deslippe, J., Park, C. H., Cohen, M. L. & Louie, S. G. Excitonic Effects on the Optical Response of Graphene and Bilayer Graphene. *Phys. Rev. Lett*. **103,** (2009).

41. Mannix, A. J., Zhou, X.-F., Kiraly, B., Wood, J. D., Alducin, D., Myers, B. D., Liu, X., Fisher, B. L., Santiago, U., Guest, J. R., Yacaman, M. J., Ponce, A., Oganov, A. R., Hersam, M. C. & Guisinger, N. P. Synthesis of borophenes: Anisotropic, two-dimensional boron polymorphs. *Science (80-.).* **350,** 1513–1516 (2015).

42. Zhang, Z., Mannix, A. J., Hu, Z., Kiraly, B., Guisinger, N. P., Hersam, M. C. & Yakobson, B. I. Substrate-Induced Nanoscale Undulations of Borophene on Silver. *Nano Lett*. **16,** 6622–6627 (2016).

43. Stokes, H. T. & Hatch, D. M. FINDSYM: program for identifying the space-group symmetry of a crystal. *J. Appl. Crystallogr*. **38,** 237–238 (2005).

44. Hohenberg, P. & Kohn, W. Inhomogeneous Electron Gas. *Phys. Rev*. **136,** 864-- 71 (1964).

45. Kohn, W. & Sham, L. J. Quantum Density Oscillations In An Inhomogeneous Electron Gas. *Phys. Rev. A* **137,** 1697–1705 (1965).

46. Hybertsen, M. S. & Louie, S. G. Electron correlation in semiconductors and insulators: Band gaps and quasiparticle energies. *Phys. Rev. B* **34,** 5390–5413 (1986).

47. Onida, G., Reining, L. & Rubio, A. Electronic excitations: density-functional versus many-body Green's-function approaches. *Rev. Mod. Phys*. **74,** 601–659 (2002).

48. Louie, S. G. in *Concept. Found. Mater. Stand. Model Ground- Excit. Prop*. (ed. Science, S. G. L. and M. L. C. B. T.-C. C. of C. M.) **Volume 2,** 9–53 (Elsevier, 2006).

49. Giustino, F., Cohen, M. L. & Louie, S. G. Electron-phonon interaction using Wannier

functions. *Phys. Rev. B* **76,** 165108 (2007).

50. Deslippe, J., Samsonidze, G., Strubbe, D. A., Jain, M., Cohen, M. L. & Louie, S. G. BerkeleyGW: A massively parallel computer package for the calculation of the quasiparticle and optical properties of materials and nanostructures. *Comput. Phys. Commun.* **183,** 1269–1289 (2012).

51. Qiu, D. Y., da Jornada, F. H. & Louie, S. G. Screening and many-body effects in two-dimensional crystals: Monolayer ${\mathrm{MoS}}_{2}$. *Phys. Rev. B* **93,** 235435 (2016).

52. Deslippe, J., Spataru, C. D., Prendergast, D. & Louie, S. G. Bound Excitons in Metallic Single-Walled Carbon Nanotubes. *Nano Lett.* **7,** 1626–1630 (2007).

53. Wang, F., Cho, D. J., Kessler, B., Deslippe, J., Schuck, P. J., Louie, S. G., Zettl, A., Heinz, T. F. & Shen, Y. R. Observation of excitons in one-dimensional metallic single-walled carbon nanotubes. *Phys. Rev. Lett.* **99,** 1–4 (2007).

54. Yang, L., Park, C.-H., Son, Y.-W., Cohen, M. L. & Louie, S. G. Quasiparticle Energies and Band Gaps in Graphene Nanoribbons. *Phys. Rev. Lett.* **99,** 186801 (2007).

55. Peng, B., Zhang, H., Shao, H., Xu, Y., Zhang, R. & Zhu, H. The electronic, optical, and thermodynamic properties of borophene from first-principles calculations. *J. Mater. Chem. C* **4,** 3592–3598 (2016).

56. Trevisanutto, P. E., Giorgetti, C., Reining, L., Ladisa, M. & Olevano, V. Ab Initio. *Phys. Rev. Lett.* **101,** 226405 (2008).

57. Noffsinger, J., Giustino, F., Malone, B. D., Park, C.-H., Louie, S. G. & Cohen, M. L. EPW: A program for calculating the electron–phonon coupling using maximally localized Wannier functions. *Comput. Phys. Commun.* **181,** 2140–2148 (2010).

58. Poncé, S., Margine, E. R., Verdi, C. & Giustino, F. EPW: Electron–phonon coupling, transport and superconducting properties using maximally localized Wannier functions. *Comput. Phys. Commun.* **209,** 116–133 (2016).

59. Park, C., Giustino, F., Spataru, C. D., Cohen, M. L. & Louie, S. G. First-Principles Study of Electron Linewidths in Graphene. *Phys. Rev. Lett.* **102,** 76803 (2009).

60. Park, C., Giustino, F., Cohen, M. L. & Louie, S. G. Velocity Renormalization and Carrier Lifetime in Graphene from the Electron-Phonon Interaction. *Phys. Rev. Lett.* **99,** 86804 (2007).

61. Giannozzi, P., Baroni, S., Bonini, N., Calandra, M., Car, R., Cavazzoni, C., Ceresoli, D., Chiarotti, G. L., Cococcioni, M., Dabo, I., Dal Corso, A., de Gironcoli, S., Fabris, S., Fratesi, G., Gebauer, R., Gerstmann, U., Gougoussis, C., Kokalj, A., Lazzeri, M., Martin-Samos, L., Marzari, N., Mauri, F., Mazzarello, R., Paolini, S., Pasquarello, A., Paulatto, L., Sbraccia, C., Scandolo, S., Sclauzero, G., Seitsonen, A. P., Smogunov, A., Umari, P. & Wentzcovitch, R. M. QUANTUM ESPRESSO: a modular and open-source software project for quantum simulations of materials. *J. Phys. Condens. Matter* **21,** 395502 (2009).

62. Troullier, N. & Martins, J. L. Efficient pseudopotentials for plane-wave calculations. *Phys. Rev. B* **43,** 1993–2006 (1991).

63. Pizzi, G., Volja, D., Kozinsky, B., Fornari, M. & Marzari, N. BoltzWann: A code for the evaluation of thermoelectric and electronic transport properties with a maximally-localized Wannier functions basis. *Comput. Phys. Commun.* **185,** 422–429 (2014).

64. Bernardi, M., Palummo, M. & Grossman, J. C. Extraordinary Sunlight Absorption and One Nanometer Thick Photovoltaics Using Two-Dimensional Monolayer Materials. *Nano Lett.* **13,** 3664–3670 (2013).

65. Yeh, P. *Optical Waves in Layered Media*. (Wiley, 2005).

66. Yeh, P. Optics of anisotropic layered media: A new 4 × 4 matrix algebra. *Surf. Sci.* **96,** 41–53 (1980).

67. Bolla, L. EMPy Electromagnetic Python. (2017). at <http://lbolla.github.io/EMpy/>

68. Lumerical Solutions, Inc. at <http://www.lumerical.com/tcad-products/fdtd/>

SYNOPSYS TOC